ACS Catalysis

Research Article

Cite This: ACS Catal. 2017, 7, 7718-7725

pubs.acs.org/acscatalysis

Active Role of Phosphorus in the Hydrogen Evolving Activity of Nickel Phosphide (0001) Surfaces

Robert B. Wexler,[†] John Mark P. Martirez,[‡] and Andrew M. Rappe*[,†]

[†]Department of Chemistry, University of Pennsylvania, Philadelphia, Pennsylvania 19104-6323, United States

[‡]Department of Mechanical and Aerospace Engineering, Princeton University, Princeton, New Jersey 08544, United States

Supporting Information

ABSTRACT: Optimizing catalysts for the hydrogen evolution reaction (HER) is a critical step toward the efficient production of $H_2(g)$ fuel from water. It has been demonstrated experimentally that transition-metal phosphides, specifically nickel phosphides Ni_2P and Ni_5P_4, efficiently catalyze the HER at a small fraction of the cost of archetypal Pt-based electrocatalysts. However, the HER mechanism on nickel phosphides remains unclear. We explore, through density functional theory with thermodynamics, the aqueous reconstructions of $Ni_2P(0001)$ and $Ni_5P_4(0001)/(000\bar{1})$, and we find that the surface P content on $Ni_2P(0001)$ depends on the applied potential, which has not been considered previously. At $-0.21\ V \geq U \geq -0.36\ V$ versus the standard hydrogen electrode and pH = 0, a PH_x-enriched Ni_3P_2 termination of $Ni_2P(0001)$ is found to be most stable, consistent with its P-rich ultrahigh-vacuum reconstructions. Above and below this potential range, the stoichiometric Ni_3P_2 surface is instead passivated by H at the Ni_3-hollow sites. On the other hand, $Ni_5P_4(000\bar{1})$ does not favor additional P. Instead, the Ni_4P_3 bulk termination of $Ni_5P_4(000\bar{1})$ is passivated by H at both the Ni_3 and P_3-hollow sites. We also found that the most HER-active surfaces are Ni_3P_2+P+(7/3)H of $Ni_2P(0001)$ and Ni_4P_3+4H of $Ni_5P_4(000\bar{1})$ due to weak H adsorption at P catalytic sites, in contrast with other computational investigations that propose Ni as or part of the active site. By looking at viable catalytic cycles for HER on the stable reconstructed surfaces, and calculating the reaction free energies of the associated elementary steps, we calculate that the overpotential on the Ni_4P_3+4H surface of $Ni_5P_4(000\bar{1})$ (−0.16 V) is lower than that of the Ni_3P_2+P+(7/3)H surface of $Ni_2P(0001)$ (−0.21 V). This is due to the abundance of P_3-hollow sites on Ni_5P_4 and the limited surface stability of the P-enriched $Ni_2P(0001)$ surface phase. The trend in the calculated catalytic overpotentials, and the potential-dependent bulk and surface stabilities explain why the nickel phosphides studied here perform almost as well as Pt, and why Ni_5P_4 is more active than Ni_2P toward HER, as is found in the experimental literature. This study emphasizes the importance of considering aqueous surface stability in predicting the HER-active sites, mechanism, and overpotential, and highlights the primary role of P in HER catalysis on transition-metal phosphides.

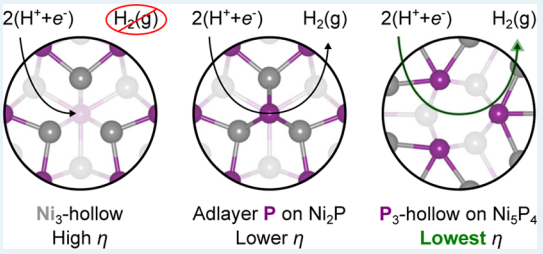

KEYWORDS: *electrocatalysis, hydrogen evolution, metal phosphides, nickel phosphides, density functional theory, aqueous surface phase diagram*

INTRODUCTION

Electrical energy produced from renewable sources (e.g., solar cells) can be used to split water to produce fuel (H_2). The cathode half-reaction of water splitting is the hydrogen evolution reaction (HER), which can be performed in both acidic (shown below) and to some extent in basic aqueous media:

$$2H^+ + 2e^- \rightleftharpoons H_2(g) \quad (1)$$

Pt is currently considered as the benchmark catalyst for the HER; however, it is both scarce and expensive.[1] This has motivated many scientists in the past decade to search for earth-abundant, cheap alternatives to Pt as electrocatalysts for the HER.[2,3]

There are two well-known mechanisms for the HER: Volmer−Tafel (VT) and Volmer−Heyrovsky (VH).[4−10] Their chemical representations are as follows:

$$H^+ + S + e^- \rightleftharpoons S{-}H \quad \text{(Volmer step)} \quad (2)$$

$$S{-}H + S'{-}H \rightleftharpoons S/S' + S'/S{-}H_2 \quad \text{(Tafel step)} \quad (3)$$

$$S{-}H + H^+ + e^- \rightleftharpoons S{-}H_2 \quad \text{(Heyrovsky step)} \quad (4)$$

$$S{-}H_2 \rightleftharpoons S + H_2(g) \quad (5)$$

Both mechanisms start with the Volmer step, where one H binds to a site (S) on the electrocatalyst surface. From here, the reaction can proceed in two different ways. Either another H will bind at a separate site (Tafel step), where S and S′ may or may not be of the same type, or directly on top of an adsorbed H forming an H_2 complex (Heyrovsky step). Both the Tafel

Received: August 14, 2017
Revised: September 20, 2017
Published: September 26, 2017

DOI: 10.1021/acscatal.7b02761
ACS Catal. 2017, 7, 7718−7725

and Heyrovsky steps are followed by the desorption of $H_2(g)$ or alternatively, lead to direct desorption of the molecule.

A few potential substitutes for Pt HER electrocatalysts are molybdenum sulfides,[2,11−24] molybdenum and tungsten carbides,[25−35] nitrides,[36−42] and nickel and cobalt phosphides.[43−51] The hydrogen evolution activity of $Ni_2P(0001)$ was originally predicted computationally[43] and then subsequently demonstrated experimentally.[44] It was proposed that the presence of P deactivates Ni and decreases the number of metal-hollow sites (the so-called "ensemble effect") while also providing weak binding for H at Ni−P bridge sites.[45] The electrostatic attraction between adsorbed $H^{\delta+}$ (at Ni−P bridge sites) and $H^{\delta-}$ (at trinuclear Ni_3-hollow sites) was proposed to facilitate HER on Ni_2P.[44]

Surface phase stability is of the utmost importance in predicting the performance of heterogeneous catalysts.[52−62] Different surface structures give rise to different sites for H adsorption, which may lead to different HER mechanisms and overpotentials. Therefore, it is essential to determine the structure and composition of the catalyst surface(s) under fabrication and operating conditions. Ni_2P has two bulk layers, Ni_3P and Ni_3P_2, along the crystal's (0001) axis; accordingly there are two bulk-like terminations: Ni_3P and Ni_3P_2. DFT calculations predict that the latter is more stable under Ni_2P bulk formation conditions.[63] Scanning tunneling microscopy (STM) and dynamic low-energy electron diffraction (LEED) experiments reveal that nonstoichiometric additional P covers ≈80% of this surface; hereafter, the surface found experimentally is denoted as $Ni_2P(s)/Ni_3P_2(0001)$+P (note that the naming scheme we adopt here is bulk/surface+adlayer where each term is the empirical formula).[64−68] Calculated adsorption energies for H at low coverage on different sites of $Ni_2P(s)/Ni_3P_2(0001)$+P show that H prefers to bind on these P adatoms.[46] We recently studied the reconstructions of both $Ni_2P(0001)$ and $Ni_5P_4(0001)/(000\bar{1})$ surfaces with DFT and discovered that the most stable terminations, subject to an inert environment, are P-enriched.[52] We predict[52] that $Ni_2P(0001)$ prefers a P-covered reconstruction of the Ni_3P_2 termination that is consistent with STM and LEED experiments in the literature.[64−68] Ni_5P_4 has three bulk layers along the (0001) and $(000\bar{1})$ axes: Ni_4P_3, Ni_3P_3, and Ni_3P_2. $Ni_5P_4(0001)/(000\bar{1})$ favors P-enrichment of the Ni_4P_3 and Ni_3P_3 terminations. Ni_3- and P_3-hollow sites, the latter of which are only present on $Ni_5P_4(s)/Ni_4P_3(0001)/(000\bar{1})$, bind additional P.

Recently, Ni_5P_4 was synthesized and was shown to exhibit exceptional, Pt-level performance for HER at pH ≈ 0 and applied potentials ranging from U = 0 V to −0.1 V vs the standard hydrogen electrode (SHE).[48] The superior performance of Ni_5P_4 was attributed to a higher positive charge on Ni atoms and to the ensemble effect of P, where the number of Ni_3-hollow sites that bind H very strongly is decreased due to the abundance of P, which therefore leads to more thermoneutral adsorption.[43,45,49] Additionally, it was shown that monodisperse Ni_5P_4 nanocrystals have higher surface area and greater stability in acidic media than Ni_2P. In this work, we only consider Ni_2P and Ni_5P_4 because they are experimentally demonstrated to be the most HER-active nickel phosphide polymorphs.[49,69,70] Additionally, these two compounds do not have strong differences between their crystal structures and structural motifs in the bulk, and both compounds also have comparable electronic conductivities.[64,71,72] Therefore, conclusions on their relative HER activities based on the compositional and structural properties of their surfaces, as well as the relative stabilities of their bulk and surfaces, can be made. A better understanding of the atomistic mechanism of the HER for various Ni phosphide systems will accelerate the design and fabrication of robust HER electrocatalysts.

To address this need, we apply DFT calculations and thermodynamics to predict the most stable surface phases under normal synthetic conditions and in an electrochemical environment, that is, aqueous solution at specified pH and applied potential U (hereafter U is implicitly relative to SHE). Each of the phosphides we model has been electrochemically investigated in aqueous solution[44,48] and is found to be stable. Thus, we model the catalytic properties of each bulk phase and evaluate which surfaces are responsible for their respective activities. We calculate the free energy of reaction of the elementary steps involved in the electrochemical HER via first-principles, and consequently, we reveal the lowest-energy pathways on $Ni_2P(0001)$ and $Ni_5P_4(0001)/(000\bar{1})$.

METHODS

First-Principles Calculations. DFT[73,74] calculations were carried out using the Quantum ESPRESSO (version 5.1) software.[75] Geometric relaxation of the bulk and surface structures was performed until changes in the total energy and force were less than 1.4×10^{-3} eV/cell and 2.6×10^{-2} eV/Å respectively. Optimized,[76] norm-conserving, designed nonlocal[77] pseudopotentials were constructed using the OPIUM (version 3.7) software[78] to replace the core electrons and nucleus with a smoother, effective potential. We used the generalized gradient approximation (GGA) as formulated by Perdew, Burke, and Ernzerhof (PBE) to calculate electron exchange and correlation energies.[79] The valence orbital wave functions were expanded in a plane-wave basis with a cutoff energy of 680 eV. Gaussian electronic smearing of 0.07 eV was applied to the band occupations near the Fermi energy to improve electronic k-point convergence. We used the semi-empirical DFT-D2 method[80] to include van der Waals (vdW) interactions, which are vital for modeling catalytic transformations.[81,82]

Bulk lattice constants were also relaxed with a pressure convergence threshold of 6.3×10^{-6} eV/Å^3. The total energies of bulk Ni_2P and Ni_5P_4 were found to be converged with 5 × 5 × 6 and 5 × 5 × 4 k-point grids respectively, offset along k_z. Calculated lattice constants and formation energies of Ni(s), P(s,white), $Ni_2P(s)$, and $Ni_5P_4(s)$ are found to be in good agreement with experimental values.[52] Slab models for $Ni_2P(0001)$ and $Ni_5P_4(0001)/(000\bar{1})$ were generated with $\sqrt{3} \times \sqrt{3}\ R30°$ surface unit cells and ≈25 Å of vacuum space separating layers. Accordingly, the k-point grid was reduced to 3 × 3 × 1. A dipole correction was added to the center of the vacuum region to cancel any artificial electric fields between the slabs.[83] Vibrational frequencies of adsorbates and surface atoms directly coupled to them were calculated (from truncated Hessian matrices) using density functional perturbation theory (DFPT). The charge densities used for these calculations were obtained by lowering the total energy convergence threshold for SCF calculations from 1.4×10^{-5} eV/cell for geometry relaxations to 1.4×10^{-9} eV/cell.

Theory. In order to accurately model catalysis, it is necessary to construct a realistic model of the surface under experimental conditions, i.e. in aqueous solution with electrochemical driving forces, pH and U.[84] This can be achieved by considering the equilibrium between surface atoms and adsorbates, and their aqueous counterparts. When a surface is

DOI: 10.1021/acscatal.7b02761
ACS Catal. 2017, 7, 7718−7725

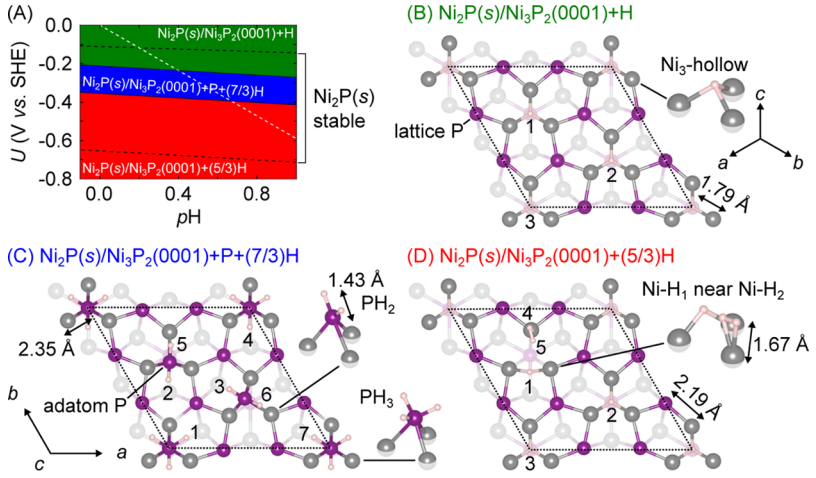

Figure 1. (A) Surface phase diagram of $Ni_2P(0001)$ in equilibrium with 1 M Ni^{2+} or Ni(s), and 1 M PH_3 or 1 M H_3PO_4 at 298.15 K. (B)−(D) show the evolution of the surface through adsorption−desorption equilibrium of P. P dissolves off the surface as phosphates (B). As the potential is lowered it redeposits as phosphines (C), up to a point where PH_3 becomes very soluble and re-exposes the Ni sites for H to bind (D). Average bond lengths are indicated.

in contact with an aqueous solution, the surface can lose atoms to or gain atoms from the solution. The chemical equation defining the equilibrium between a surface and aqueous solution where atom A is being exchanged is as follows

$$S{-}A + n_w H_2O \rightleftharpoons S + [H_xAO_y]^z + n_H H^+ + n_e e^- \quad (6)$$

where S is the surface, n_w is the number of water molecules needed to oxidize (reduce) and/or solvate A in the solution, $[H_xAO_y]^z$ is the most stable aqueous phase of A, z is the charge of the A-complex which can either be positive, negative, or zero, n_H is the number of protons formed, and n_e is the number of electrons released. Note that the latter two can be negative in which case proton(s) and electron(s) are gained to form $[H_xAO_y]^z$. The free-energy change for this dissolution reaction of one A ion is

$$\Delta G_{A,diss} = (G_S - G_{SA}) + (G_{H_xAO_y^z} + n_H G_H + n_e G_e - n_w G_{H_2O}) \quad (7)$$

We can rewrite $\Delta G_{A,diss}$ with respect to the standard state of A, A(std), as

$$\Delta G_{A,diss} = (G_S + G_{A(std)} - G_{SA}) + (G_{[H_xAO_y]^z} + n_H G_H + n_e G_e - G_{A(std)} - n_w G_{H_2O}) \quad (8)$$

Note here we simply add $G_{A(std)}$ to the first term and subtract it from the second term. We define the first term as the differential desorption (dsrp) free energy ΔG_{dsrp} for A to leave the surface and form A(std). We re-express the second term with respect to the standard oxidation/reduction free energy $\Delta G^\circ_{A(std)/H_xAO_y^z}$ of A(std) to form $[H_xAO_y]^z$ (see additional theoretical details and Table S1 in the Supporting Information). Our final expression is

$$\Delta G_{A,diss} = \Delta G_{dsrp} + \Delta G^\circ_{A(std)/H_xAO_y^z} + k_B T \ln a_{H_xAO_y^z} - 2.303 n_H k_B T pH - n_e q_e U \quad (9)$$

The last three terms represent the deviation of the chemical potentials due to concentrations of the aqueous species: $H_xAO_y^z$, and H^+ from the standard condition, and of the electronic energy relative to SHE:

$$\Delta G_{A,diss} = \Delta G_{dsrp} + \Delta G^\circ_{A(std)/H_xAO_y^z} + \Delta\mu_{H_xAO_y^z} + n_H \Delta\mu_H + n_e \Delta\mu_e \quad (10)$$

where $\Delta\mu_{H_xAO_y^z} = k_B T \ln a_{H_xAO_y^z}$, $\Delta\mu_H = -2.303 k_B T pH$, and $\Delta\mu_e = -q_e U$. These terms can be thought of as knobs that control the chemical potentials of $H_xAO_y^z$, protons, and electrons, respectively. We calculated ΔG_{dsrp} using DFT and evaluated the relative stability of different surface phases of Ni_2P and $Ni_5P_4(0001)$ by modeling reactions represented in eq 6. We investigated various H coverages on each surface reconstruction, up to 7 H atoms per 3 surface unit cells (θ = 7/3 or 1.32 nmol H/cm^2, where the surface area, $A = 2.93 \times 10^{-15}$ cm^2/(1 × 1) surface) for Ni_2P and θ = 14/3 H atoms (2.00 nmol H/cm^2, where $A = 3.87 \times 10^{-15}$ cm^2/(1 × 1) surface) for Ni_5P_4, in increments of $\Delta\theta$ = 1/3 (0.19 nmol H/cm^2 for Ni_2P and 0.14 nmol H/cm^2 for Ni_5P_4). The aforementioned maximum coverages are the highest possible coverages for which H adsorption is preferred to physisorbed H_2. We found that the thermodynamically optimal coverages in the relevant range of pH and applied potential are within the maximum coverages explored. We computed their free energies using eq 10 relative to the Ni_3P_2+P and bulk Ni_4P_3 terminations for Ni_2P and Ni_5P_4 surfaces, respectively (see Tables S2−4 in the Supporting Information).

We generate Pourbaix diagrams, which map the equilibrium phases of an aqueous electrochemical system, for Ni and P, by calculating $\Delta G^\circ_{A(std)/H_xAO_y^z}$ and identifying the most stable species for given pH and U (see Figure S1 in the Supporting Information). An expression for the complete dissolution of the bulk Ni_aP_b phase can be derived following eqs 6−10:

$$\Delta G_{Ni_aP_b,diss} = -\Delta G^f_{Ni_aP_b} + a\Delta G_{Ni(s)/H_xNiO_y^z} + b\Delta G_{P(s,white)/H_xPO_x^z} \quad (11)$$

where $\Delta G^f_{Ni_aP_b}$ is the free energy of formation of Ni_aP_b. The stability criterion is $\Delta G_{Ni_aP_b,diss} \geq 0$, and thus, we define the bulk stability boundary as

DOI: 10.1021/acscatal.7b02761
ACS Catal. 2017, 7, 7718−7725

$$\Delta G^{f}_{Ni_aP_b} \leq a\Delta G_{Ni(s)/H_xNiO_y^z} + b\Delta G_{P(s,white)/H_xPO_y^z} \quad (12)$$

The bulk phase diagrams of Ni_2P and Ni_5P_4 are shown in Figure S2 in the Supporting Information. Finally, we calculated free energies of hydrogen adsorption (see reaction in eq 2)

$$\Delta G_{ads} = G(n_H + 1) - G(n_H) - G(H^+ + e^-) \quad (13)$$

at 298.15 K, pH = 0, and U = 0 V.

RESULTS AND DISCUSSION

Structure and Aqueous Stability of $Ni_2P(0001)$ Surfaces. For this study, we consider an acidic aqueous environment (pH = −0.1−1, which corresponds to typical experimental conditions for HER in acid, i.e. $[H_2SO_4]$ = 1−0.1 M)[44,48] and calculate the free energy of $Ni_2P(0001)$ surfaces in equilibrium with 1 M Ni^{2+} or Ni(s), and 1 M PH_3 or 1 M H_3PO_4 at 298.15 K (see Table S2 in the Supporting Information). For the purpose of our discussion, we choose the standard concentration of 1 M for the aqueous species as a suitable reference to define the bulk and surface phase stability boundaries. The results for 0.01 and 0.001 M concentrations are plotted in Figure S6 in the Supporting Information, where we show that qualitatively the observed trends in stability and reactivity are unaffected, while quantitatively, the upper bound for the applied potential where the phases are stable varies by 0.02−0.05 V. In the regions of U and pH where solubility is greater than 1M, it is reasonable to conclude that the catalyst would no longer be practical, as it would experience significant material loss during catalysis and after prolonged use (see Figure S2 for the calculated solubility of the bulk as a function of U and pH). Also, we note that the overpotential calculated for an HER elementary step for a given surface is independent of these concentrations. Figure 1A shows the phase diagram for the (0001) surface of Ni_2P. At U > −0.21 V, $Ni_2P(s)/Ni_3P_2(0001)$ with one H per surface unit cell, hereafter denoted as $Ni_2P(s)/Ni_3P_2(0001)$+H, is the dominant surface phase. The $\sqrt{3} \times \sqrt{3}$ $R30°$ surface has one H bonded to each Ni_3-hollow site (labeled 1−3 in Figure 1B). Ni_3-hollow sites strongly bind H, with an adsorption free energy (see eq 13) of −0.47 eV/H. We summarize ΔG_{ads} for different sites on $Ni_2P(0001)$ and $Ni_5P_4(000\bar{1})$ in Table 1.

Table 1. Free Energy of H Adsorption on Selected Surface Sites of $Ni_2P(0001)$ and $Ni_5P_4(000\bar{1})$ in Equilibrium with 1 M Ni^{2+} or Ni(s), and 1 M PH_3 or 1 M H_3PO_4 at 298.15 K, U = 0 V, and pH = 0

bulk	surface	orientation	active site	ΔG_{ads} (eV)
Ni_2P	Ni_3P_2+H	(0001)	Ni_3-hollow	−0.47
Ni_2P	Ni_3P_2+P+(7/3)H	(0001)	adatom P	0.01 to 0.14
Ni_5P_4	Ni_4P_3+4H	$(000\bar{1})$	Ni_3-hollow	−0.57
Ni_5P_4	Ni_4P_3+4H	$(000\bar{1})$	P_3-hollow	−0.27 to −0.06

For −0.21 V ≥ U ≥ −0.36 V, a P-enriched phase, $Ni_2P(s)/Ni_3P_2(0001)$+P+(7/3)H is most stable. Aqueous P reacts with the surface, replacing the H atom at each Ni_3-hollow site with P. This surface is similar to the UHV reconstruction $Ni_2P(s)/Ni_3P_2(0001)$+P,[52] but here P-adatoms are also hydrogenated. More specifically, one adatom P forms a surface PH_3 moiety, whereas the other two form PH_2 for a total of seven H atoms (labeled 1−7 in 1C) per $\sqrt{3} \times \sqrt{3}$ $R30°$ surface unit cell. These units, with an average P−H bond length of 1.43 Å, form the precursor for phosphine molecule ($\bar{d}_{PH}$ = 1.42 Å[85]) desorption, which occurs at U < −0.36 V. The side view in Figure 1B reveals that P is exposed and able to react with more H than the $Ni_2P(s)/Ni_3P_2(0001)$ surface. The bond length between in-plane Ni and P is 2.19 Å, whereas the bond length between Ni and adatom P is elongated (2.35 Å), signaling a weaker bond. As such, adatom P is able to form a stronger bond with H (ΔG_{ads} = 0.05 eV/H) than the lattice P (ΔG_{ads} = 0.27 eV/H). H-binding is much weaker on adatom P sites than Ni_3-hollow sites, in agreement with the literature.[46]

Below U = −0.36 V, PH_3 desorbs and re-exposes the Ni_3-hollow sites again for H to bind, one H per Ni_3. Two additional H adsorb on the surface (labeled 4 and 5 in Figure 1D) forming $Ni_2P(s)/Ni_3P_2(0001)$+(5/3)H, where Ni forms a complex with H_2, pushing the central H to a Ni-bridge site. The average Ni−H bond length involving atomic H decreases from 1.79 Å on $Ni_2P(s)/Ni_3P_2(0001)$+H to 1.67 Å on $Ni_2P(s)/Ni_3P_2(0001)$+(5/3)H because of the reduced coordination of number of H. The H−H bond length (0.82 Å) is only slightly larger than that of $H_2(g)$ (0.74 Å[86]), highlighting the weak adsorption of this species.

Structure and Aqueous Stability of $Ni_5P_4(000\bar{1})$ Surfaces. For $Ni_5P_4(000\bar{1})$, only two different surface phases are observed under acidic (pH = −0.1−1), reducing (U = 0.0 to −0.8 V) conditions (see Figure 2A). For $U \geq$ −0.37 V, the predominant surface phase is $Ni_5P_4(s)/Ni_4P_3(000\bar{1})$+4H. The structure of this surface is shown in Figure 2B, and it consists of repeating Ni_3- and P_3-hollows connected by central Ni atoms. The P_3-hollow sites are unique to Ni_5P_4 and specifically the Ni_4P_3 termination. There are two different types of Ni−P bonds, one with a bond length of 2.09 Å between P and the central Ni and another with a bond length of 2.26 Å between P and a Ni from a Ni_3-hollow. The average of these two Ni−P bond lengths is near the bond length between in-plane Ni and P on $Ni_2P(s)/Ni_3P_2(0001)$ surfaces. Three H atoms adsorb, per $\sqrt{3} \times \sqrt{3}$ supercell, one at each Ni_3-hollow with equal bonding contributions from all three Ni atoms and an average bond length of 1.74 Å. H binding is stronger at the Ni_3-hollow site on $Ni_5P_4(s)/Ni_4P_3(000\bar{1})$+4H, with an average adsorption free energy of −0.57 eV/H. Nine additional H atoms per supercell adsorb, three per P_3-hollow site (circled and shaded in light purple in in Figure 2B). Each H makes a single P−H bond of length 1.42 Å, and the H atoms point toward the center of the P_3-hollow. We find a positive correlation between ΔG_{ads} and H coverage (n_H) at the P_3-hollow sites (see Figure 3), and we attribute this to repulsive interactions between H adsorbates. As H coverage at P_3-hollows increases, surface H species are forced into close proximity, thereby increasing the P−P−H angle (see inset in Figure 3), destabilizing H adsorption, and shifting it toward thermoneutrality. This coverage-dependent chemisorption energy is the key feature that makes P_3-hollows superior to other P-based active sites. At more negative potentials, U < −0.37 V, two additional H atoms per supercell bind to one of the Ni_3-hollows, generating a Ni−H_2 complex (d_{HH} = 0.86 Å) identical to that on $Ni_2P(s)/Ni_3P_2(0001)$+(5/3)H, as shown in Figure 2C. Consequently, there are three domains of binding energy on Ni_5P_4 (colored red, blue, and green in Figure 3). The maximum coverage of $Ni_5P_4(000\bar{1})$ is 1.5 times larger than that of $Ni_2P(0001)$. We also consider P-enriched $(000\bar{1})$ surfaces in our stability analysis (see Table S4 in the Supporting Information) but find that they are not stable in acidic aqueous media, unlike in $Ni_2P(0001)$, where an adlayer of P forms. P_3-hollows, however, are more advantageous for the HER than adatom P because they exist at less negative overpotentials.

DOI: 10.1021/acscatal.7b02761
ACS Catal. 2017, 7, 7718−7725

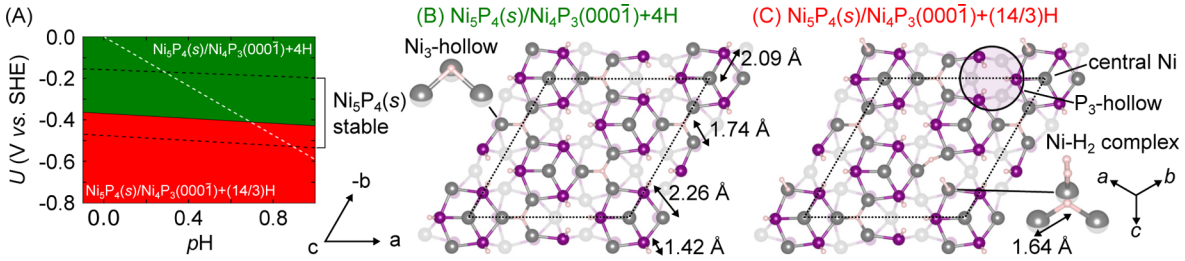

Figure 2. (A) Surface phase diagram of $Ni_5P_4(s)/Ni_4P_3(000\bar{1})$ in equilibrium with 1 M Ni^{2+} or Ni(*s*), and 1 M PH_3 or 1 M H_3PO_4 at 298.15 K. (B), (C) show the evolution of the surface through adsorption−desorption equilibrium of H. H binds at the Ni_3- and P_3-hollow sites, one H per Ni_3 and three H per P_3. As the potential is lowered, two additional H adsorb at the Ni_3-hollow site, forming a Ni−H_2 complex.

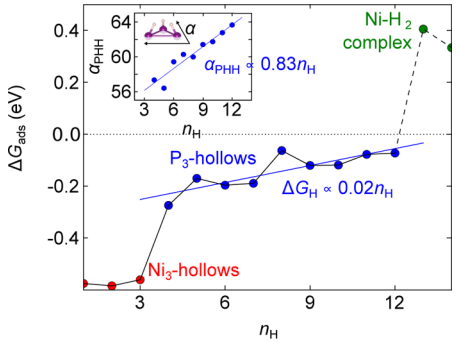

Figure 3. Free energy of H adsorption as a function of H coverage (n_H) on $Ni_5P_4(s)/Ni_4P_3(000\bar{1})$ in equilibrium with 1 M Ni^{2+} or Ni(*s*), and 1 M PH_3 or 1 M H_3PO_4 at 298.15 K, U = 0 V, and pH = 0. Colors differentiate H binding sites. Solid (dashed) lines connect coverages where hydrogen adsorption is exergonic (endergonic). Dotted line at ΔG_H = 0 eV corresponds to thermoneutral H adsorption. We fit ΔG_H at P_3-hollow sites to a simple linear model to quantify the destabilization of P−H with increasing n_H. Inset is a plot of the P−P−H angle vs n_H.

We defer our discussion of $Ni_5P_4(0001)$ surfaces to the Supporting Information (see Figure S3) because the $(000\bar{1})$ surfaces offer lower HER overpotentials, which now will be discussed.

HER Mechanism of $Ni_2P(0001)$ and $Ni_5P_4(000\bar{1})$ Surfaces. In general, the most efficient catalytic mechanisms occur between nearly isoenergetic surface phases, such that each step in the reaction is thermoneutral or low-energy. For electrochemical reactions that do not occur spontaneously, an applied potential can be used to drive the reaction. Here, we define the overpotential η as the potential required to make all elementary steps in the HER spontaneous and ensure catalyst stability, since a prerequisite for catalysis is a regenerable surface that supports it. In the following discussion on the mechanism of the HER, the predictions we make satisfy these criteria.

The HER mechanism on Ni_2P is still debated in the literature. Computational studies have focused on stoichiometric Ni_2P surfaces, with none considering the influence of surface reconstruction driven by the aqueous phase in contact with the catalyst. There are two main proposals for the HER active site on Ni_2P: cooperative Ni_3-hollow and Ni−P bridge sites on the (0001) facet,[43] and Ni−Ni bridge sites on the $(\bar{1}\bar{1}20)$ and $(11\bar{2}0)$ surfaces.[47] Here, we present alternative mechanisms that exhibit the lowest overpotentials for HER on the (0001) surfaces of Ni_2P and Ni_5P_4. A less favorable mechanism on $Ni_5P_4(0001)$ is reported in the Supporting Information.

For $Ni_2P(0001)$, we find that the H-covered, P-enriched Ni_3P_2+P+(7/3)H surface offers the lowest overpotential for HER via the Volmer−Heyrovsky mechanism. Figure 4A shows

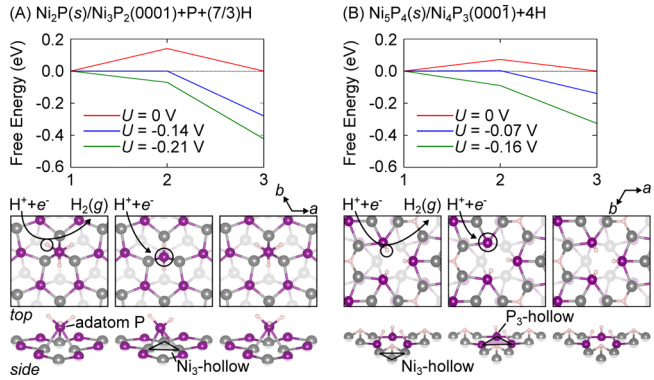

Figure 4. Free energy and structures of intermediates in the HER for (A) $Ni_2P(0001)$ and (B) $Ni_5P_4(000\bar{1})$ in equilibrium with 1 M Ni^{2+} or Ni(*s*), and 1 M PH_3 or 1 M H_3PO_4 at 298.15 K and pH = 0. The blue line corresponds to minimum overpotential to make the reaction spontaneous. The green line, however, corresponds to minimum overpotential to make the reaction spontaneous and ensure catalyst stability.

the free energies and structures of reaction intermediates. The first step of this reaction involves two concerted events: (a) reaction of a proton in solution and electron with H at a PH_3 moiety and (b) desorption of $H_2(g)$ to form PH_2. In the second step, the PH_3 subunit is replenished by another proton and electron. At U = 0 V, this reaction has a 0.14 eV barrier (black line in Figure 4A), and consequently, the application of −0.14 V (red line) makes each step spontaneous. Ni_3P_2+P+(7/3)H, however, is only stable for $-0.21\ V \geq U \geq -0.36$ V. Therefore, we portray an overpotential of −0.21 V (green line) for $Ni_2P(0001)$, since the reaction is limited by the stability of the active surface phase (the dominant surface at U = −0.14 V has a larger overpotential requirement, U = −0.26 V, see Figure S4 in the Supporting Information). This mechanism is different from those previously proposed in the literature for Ni_2P,[43,47] highlighting the importance of considering aqueous phase stability in the prediction of catalytic mechanisms. It was also predicted that Ni−P bridge sites on $Ni_2P(s)/Ni_3P_2(0001)$ offer weaker binding for H. However, we find that these sites are not stable.

$Ni_5P_4(000\bar{1})$ offers a surface phase that provides efficient HER catalysis, Ni_4P_3+4H. Like $Ni_2P(0001)$, this surface favors a Volmer−Heyrovsky mechanism, as shown in Figure 4B. This mechanism involves the simultaneous addition of H and abstraction of $H_2(g)$ from a P_3-hollow site followed by H

DOI: 10.1021/acscatal.7b02761
ACS Catal. 2017, 7, 7718−7725

adsorption to replenish the third H at the P_3-hollow site. At U = 0 V, this HER mechanism has a smaller barrier (0.07 eV at U = 0 V, black line in 4B) and consequently requires a smaller overpotential (−0.07 V, red line) to make each step spontaneous. Bulk $Ni_5P_4(s)$, however, is only stable with respect to dissolution for $-0.16\ V \geq U \geq -0.48\ V$ at pH = 0, whereas $Ni_2P(s)$ is stable for $-0.11\ V \geq U \geq -0.66\ V$. This prediction agrees with an experiment where it has been shown that applying negative potential (≈ −0.2 V vs RHE) suppresses degradation of Ni_5P_4.[87] For positive potentials, i.e. $U \approx 0.3$ V vs RHE, the compound dissolves with a rate of 1 ng/s/cm^2.[87] Therefore, the performance of Ni_5P_4 is expected to degrade over time for potentials higher than the stabilizing potential. Therefore, the lowest HER overpotential for $Ni_5P_4(000\bar{1})$ is −0.16 V, as the reaction is limited by the stability of bulk $Ni_5P_4(s)$. From this, we see that the $(000\bar{1})$ surfaces of Ni_5P_4 are more HER active than that of $Ni_2P(0001)$, in agreement with experimental reports.[48] If one were only to consider thermodynamic barriers associated with the catalytic cycle, $Ni_5P_4(000\bar{1})$ would still have a lower overpotential (−0.07 V) than $Ni_2P(0001)$ (−0.14 V). Since we find that the adsorption energy of H on Ni_5P_4 is nearly thermoneutral, i.e. −0.07 eV, the intrinsic activity of Ni_5P_4 should be comparable to that of Pt. However, while it is experimentally found that the overall activity of nanocrystalline Ni_5P_4 approaches that of Pt on an electrode-basis, the surface-area-normalized turnover frequency (TOF) of Pt, i.e. performance on the basis of intrinsic activity (irrespective of morphology), is 2 orders of magnitude higher than that of Ni_5P_4.[48] This apparent inconsistency between the calculated catalytic overpotential and the experimentally measured TOF can be explained by the limited aqueous stability of bulk Ni_5P_4, requiring an applied potential $U \leq -0.16$ V (higher potentials are expected to degrade the phosphides' performance). This reconciles the "apparent" intrinsic activity of Ni_5P_4 being below that of Pt, although we predict that purely on the basis of catalytic activity of the active surface, $Ni_5P_4(0001)$ is comparable to that of Pt. Synthetic methods, e.g. chemical doping, that would allow for Ni_5P_4 to be stable near 0 V vs SHE are therefore expected to lead to higher performance for the phosphide.

Since our calculations indicate that the P_3-hollow is the most active site for HER catalysis, we propose high-throughput searching for materials that express this motif. P_3-hollows form on $Ni_5P_4(s)/Ni_4P_3(000\bar{1})$ because of the high P content in Ni_5P_4 relative to other bulk nickel phosphides and the ability of bulk $P(s)$ to form stable clusters.[52] Clustering behavior in nonmetals is not unique to P, as $S(s)$ also exhibits many different allotropes with various clustering geometries. As such, we believe that multinonmetal sites in general may hold promise for HER catalysis and should be a focal point for researchers studying the HER. Another way to improve the efficiency of nickel phosphides for HER therefore would be to subtly modulate the metal−P bond strength so as to indirectly shift the free energy of H adsorption toward thermoneutrality. This opens a clear path for materials design of new materials to improve HER activity by tuning metal−P bond strength via lattice strain (e.g., epitaxial film growth) or low concentration doping/ion exchange with other elements. To date, however, there has only been one study of the relationship between Fe and Co-doping on the H adsorption free energy.[88] Since we find P to be the active site for HER on Ni_2P and Ni_5P_4, we recommend anionic substitutions for P as a more straightforward path to tune the catalytic activity,[89−91] in contrast with the transition metal substitution approach proposed recently.[88] For example, the presence of the more electronegative S can directly (through the formation of S−H) or indirectly (through modulation of the Ni−P bond strength) affect the binding of H onto the surface. Given that Ni_2P is a hydrodesulfurization catalyst,[45] surface substitution with S should be possible. Nickel phosphide HER catalysts are reported to have nearly quantitative Faradaic efficiencies.[44,92−94] Therefore, the formation of reduction side products from the electrolyte leading to the formation of reduced sulfur species is assumed not to occur and not included in our models. Further studies are necessary to develop a robust theory of chemical bonding between metal, P, and H in transition-metal phosphides, which could ultimately provide systematic guidance for designing improved HER catalysts.

CONCLUSIONS

The $(000\bar{1})$ surface of Ni_5P_4 provides lower HER overpotentials and therefore greater HER activity than $Ni_2P(0001)$, which can be attributed to the thermodynamics and structure of surface P. For $Ni_2P(0001)$, the most stable aqueous surface reconstructions are $Ni_2P(s)/Ni_3P_2(0001)+nH$ (n = 1, 5/3) and $Ni_2P(s)/Ni_3P_2(0001)+P+(7/3)H$, with the latter having an HER overpotential of −0.21 V. For Ni_5P_4, the $(000\bar{1})$ facet is more catalytically active than (0001), and the most stable aqueous reconstruction is $Ni_5P_4(s)/Ni_4P_3(000\bar{1})+nH$ (n = 4, 14/3). This surface has the lowest overpotential for HER at −0.16 V. P, and not Ni, is the most active site, with adatom P and P_3-hollows providing low overpotential HER via the Volmer−Heyrovsky mechanism on Ni_2P and Ni_5P_4 (0001) surfaces. The P_3-hollow site on $Ni_5P_4(s)/Ni_4P_3(000\bar{1})$, which is present at low overpotential and offers nearly optimal H adsorption, is the origin of the superior catalytic activity of Ni_5P_4. The structural flexibility of P, i.e. its ability to form surface adlayers (adatom P) and in-plane multi-P clusters (P_3-hollow), provides a new frontier for improving the catalytic activity of transition-metal phosphides by embarking on high-throughput computational searches for catalysts that express these motifs and modulating the interaction strength between the metal and phosphorus via strain and surface doping.

ASSOCIATED CONTENT

Supporting Information

The Supporting Information is available free of charge on the ACS Publications website at DOI: 10.1021/acscatal.7b02761.

Additional computational details, additional theoretical details, tabulated experimental standard formation free energies of solid and aqueous Ni and P species, Pourbaix diagrams for Ni and P, bulk phase diagrams for Ni_2P and Ni_5P_4, free energies of $Ni_2P(0001)$ and $Ni_5P_4(0001)/(000\bar{1})$ surfaces, structure and aqueous stability of the $Ni_5P_4(0001)$ surfaces, additional hydrogen evolution reaction mechanisms, and surface phase diagrams of $Ni_2P(0001)$ and $Ni_5P_4(000\bar{1})$ in equilibrium with different molar concentrations of solvated species (PDF)

AUTHOR INFORMATION

Corresponding Author

*E-mail: rappe@sas.upenn.edu.

ORCID

Robert B. Wexler: 0000-0002-6861-6421

DOI: 10.1021/acscatal.7b02761
ACS Catal. 2017, 7, 7718−7725

Andrew M. Rappe: 0000-0003-4620-6496

Notes

The authors declare no competing financial interest.

■ ACKNOWLEDGMENTS

R.B.W., J.M.P.M., and A.M.R. acknowledge support from the Office of Naval Research under grant number N00014-17-1-2574. The authors also acknowledge computational support from the High-Performance Computing Modernization Office and the National Energy Research Scientific Computing Center.

■ REFERENCES

(1) Marković, N.; Ross, P. N. *Surf. Sci. Rep.* **2002**, *45*, 117−229.
(2) Hinnemann, B.; Moses, P. G.; Bonde, J.; Jørgensen, K. P.; Nielsen, J. H.; Horch, S.; Chorkendorff, I.; Nørskov, J. K. *J. Am. Chem. Soc.* **2005**, *127*, 5308−5309.
(3) Greeley, J.; Jaramillo, T. F.; Bonde, J.; Chorkendorff, I.; Nørskov, J. K. *Nat. Mater.* **2006**, *5*, 909−913.
(4) Gennero de Chialvo, M. R.; Chialvo, A. *J. Electrochem. Soc.* **2000**, *147*, 1619−1622.
(5) Gennero de Chialvo, M. R.; Chialvo, A. C. *Phys. Chem. Chem. Phys.* **2004**, *6*, 4009−4017.
(6) Quaino, P. M.; Gennero de Chialvo, M. R.; Chialvo, A. C. *Phys. Chem. Chem. Phys.* **2004**, *6*, 4450−4455.
(7) Conway, B.; Bai, L. *J. Electroanal. Chem. Interfacial Electrochem.* **1986**, *198*, 149−175.
(8) Conway, B.; Bai, L. *Int. J. Hydrogen Energy* **1986**, *11*, 533−540.
(9) Zheng, Y.; Jiao, Y.; Jaroniec, M.; Qiao, S. Z. *Angew. Chem., Int. Ed.* **2015**, *54*, 52−65.
(10) Conway, B.; Tilak, B. *Adv. Catal.* **1992**, *38*, 1−147.
(11) Jaramillo, T. F.; Jørgensen, K. P.; Bonde, J.; Nielsen, J. H.; Horch, S.; Chorkendorff, I. *Science* **2007**, *317*, 100−102.
(12) Jaramillo, T. F.; Bonde, J.; Zhang, J.; Ooi, B.-L.; Andersson, K.; Ulstrup, J.; Chorkendorff, I. *J. Phys. Chem. C* **2008**, *112*, 17492−17498.
(13) Hou, Y.; Abrams, B. L.; Vesborg, P. C. K.; Björketun, M. E.; Herbst, K.; Bech, L.; Setti, A. M.; Damsgaard, C. D.; Pedersen, T.; Hansen, O.; Rossmeisl, J.; Dahl, S.; Nørskov, J. K.; Chorkendorff, I. *Nat. Mater.* **2011**, *10*, 434−438.
(14) Seger, B.; Herbst, K.; Pedersen, T.; Abrams, B.; Vesborg, P. C. K.; Hansen, O.; Chorkendorff, I. *J. Electrochem. Soc.* **2014**, *161*, H722−H724.
(15) Kibsgaard, J.; Jaramillo, T. F.; Besenbacher, F. *Nat. Chem.* **2014**, *6*, 248−253.
(16) Merki, D.; Fierro, S.; Vrubel, H.; Hu, X. *Chem. Sci.* **2011**, *2*, 1262−1267.
(17) Kibsgaard, J.; Chen, Z.; Reinecke, B. N.; Jaramillo, T. F. *Nat. Mater.* **2012**, *11*, 963−969.
(18) Li, Y.; Wang, H.; Xie, L.; Liang, Y.; Hong, G.; Dai, H. *J. Am. Chem. Soc.* **2011**, *133*, 7296−7299.
(19) Li, D. J.; Maiti, U. N.; Lim, J.; Choi, D. S.; Lee, W. J.; Oh, Y.; Lee, G. Y.; Kim, S. O. *Nano Lett.* **2014**, *14*, 1228−1233.
(20) Bonde, J.; Moses, P. G.; Jaramillo, T. F.; Nørskov, J. K.; Chorkendorff, I. *Faraday Discuss.* **2009**, *140*, 219−231.
(21) Merki, D.; Vrubel, H.; Rovelli, L.; Fierro, S.; Hu, X. *Chem. Sci.* **2012**, *3*, 2515−2525.
(22) Lukowski, M. A.; Daniel, A. S.; Meng, F.; Forticaux, A.; Li, L.; Jin, S. *J. Am. Chem. Soc.* **2013**, *135*, 10274−10277.
(23) Voiry, D.; Yamaguchi, H.; Li, J.; Silva, R.; Alves, D. C.; Fujita, T.; Chen, M.; Asefa, T.; Shenoy, V. B.; Eda, G.; Chhowalla, M. *Nat. Mater.* **2013**, *12*, 850−855.
(24) Wang, H.; Lu, Z.; Kong, D.; Sun, J.; Hymel, T. M.; Cui, Y. *ACS Nano* **2014**, *8*, 4940−4947.
(25) Vrubel, H.; Hu, X. *Angew. Chem.* **2012**, *124*, 12875−12878.
(26) Chen, W.-F.; Wang, C.-H.; Sasaki, K.; Marinkovic, N.; Xu, W.; Muckerman, J.; Zhu, Y.; Adzic, R. *Energy Environ. Sci.* **2013**, *6*, 943−951.
(27) Esposito, D. V.; Hunt, S. T.; Stottlemyer, A. L.; Dobson, K. D.; McCandless, B. E.; Birkmire, R. W.; Chen, J. G. *Angew. Chem., Int. Ed.* **2010**, *49*, 9859−9862.
(28) Wu, H. B.; Xia, B. Y.; Yu, L.; Yu, X.-Y.; Lou, X. W. D. *Nat. Commun.* **2015**, *6*, 6512.
(29) Esposito, D. V.; Hunt, S. T.; Kimmel, Y. C.; Chen, J. G. *J. Am. Chem. Soc.* **2012**, *134*, 3025−3033.
(30) Youn, D. H.; Han, S.; Kim, J. Y.; Kim, J. Y.; Park, H.; Choi, S. H.; Lee, J. S. *ACS Nano* **2014**, *8*, 5164−5173.
(31) Wan, C.; Regmi, Y. N.; Leonard, B. M. *Angew. Chem.* **2014**, *126*, 6525−6528.
(32) Esposito, D. V.; Chen, J. G. *Energy Environ. Sci.* **2011**, *4*, 3900−3912.
(33) Harnisch, F.; Sievers, G.; Schröder, U. *Appl. Catal., B* **2009**, *89*, 455−458.
(34) Yan, Y.; Xia, B.; Qi, X.; Wang, H.; Xu, R.; Wang, J.-Y.; Zhang, H.; Wang, X. *Chem. Commun.* **2013**, *49*, 4884−4886.
(35) Liu, Y.; Yu, G.; Li, G.-D.; Sun, Y.; Asefa, T.; Chen, W.; Zou, X. *Angew. Chem., Int. Ed.* **2015**, *54*, 10752−10757.
(36) Chen, W.-F.; Sasaki, K.; Ma, C.; Frenkel, A. I.; Marinkovic, N.; Muckerman, J. T.; Zhu, Y.; Adzic, R. R. *Angew. Chem., Int. Ed.* **2012**, *51*, 6131−6135.
(37) Zheng, P.; Zhao, J.; Zheng, J.; Ma, G.; Zhu, Z. *J. Mater. Chem.* **2012**, *22*, 12116−12120.
(38) Su, J.; Lu, N.; Zhao, J.; Yu, H.; Huang, H.; Dong, X.; Quan, X. *J. Hazard. Mater.* **2012**, *231*, 105−113.
(39) Ishikawa, A.; Takata, T.; Kondo, J. N.; Hara, M.; Domen, K. *J. Phys. Chem. B* **2004**, *108*, 11049−11053.
(40) Wirth, S.; Harnisch, F.; Weinmann, M.; Schröder, U. *Appl. Catal., B* **2012**, *126*, 225−230.
(41) Choi, D.; Blomgren, G. E.; Kumta, P. N. *Adv. Mater.* **2006**, *18*, 1178−1182.
(42) Choi, D.; Kumta, P. N. *Electrochem. Solid-State Lett.* **2005**, *8*, A418−A422.
(43) Liu, P.; Rodriguez, J. A. *J. Am. Chem. Soc.* **2005**, *127*, 14871−14878.
(44) Popczun, E. J.; McKone, J. R.; Read, C. G.; Biacchi, A. J.; Wiltrout, A. M.; Lewis, N. S.; Schaak, R. E. *J. Am. Chem. Soc.* **2013**, *135*, 9267−9270.
(45) Liu, P.; Rodriguez, J. A.; Asakura, T.; Gomes, J.; Nakamura, K. *J. Phys. Chem. B* **2005**, *109*, 4575−4583.
(46) Ariga, H.; Kawashima, M.; Takakusagi, S.; Asakura, K. *Chem. Lett.* **2013**, *42*, 1481−1483.
(47) Hansen, M. H.; Stern, L.-A.; Feng, L.; Rossmeisl, J.; Hu, X. *Phys. Chem. Chem. Phys.* **2015**, *17*, 10823−10829.
(48) Laursen, A. B.; Patraju, K. R.; Whitaker, M. J.; Retuerto, M.; Sarkar, T.; Yao, N.; Ramanujachary, K. V.; Greenblatt, M.; Dismukes, G. C. *Energy Environ. Sci.* **2015**, *8*, 1027−1034.
(49) Pan, Y.; Liu, Y.; Zhao, J.; Yang, K.; Liang, J.; Liu, D.; Hu, W.; Liu, D.; Liu, Y.; Liu, C. *J. Mater. Chem. A* **2015**, *3*, 1656−1665.
(50) Anantharaj, S.; Reddy, P. N.; Kundu, S. *Inorg. Chem.* **2017**, *56*, 1742−1756.
(51) Anantharaj, S.; Ede, S. R.; Sakthikumar, K.; Karthick, K.; Mishra, S.; Kundu, S. *ACS Catal.* **2016**, *6*, 8069−8097.
(52) Wexler, R. B.; Martirez, J. M. P.; Rappe, A. M. *Chem. Mater.* **2016**, *28*, 5365−5372.
(53) Kim, S.; Sinai, O.; Lee, C.-W.; Rappe, A. M. *Phys. Rev. B: Condens. Matter Mater. Phys.* **2015**, *92*, 235431.
(54) Martirez, J. M. P.; Kim, S.; Morales, E. H.; Diroll, B. T.; Cargnello, M.; Gordon, T. R.; Murray, C. B.; Bonnell, D. A.; Rappe, A. M. *J. Am. Chem. Soc.* **2015**, *137*, 2939−2947.
(55) Saidi, W. A.; Martirez, J. M. P.; Rappe, A. M. *Nano Lett.* **2014**, *14*, 6711−6717.
(56) Koocher, N. Z.; Martirez, J. M. P.; Rappe, A. M. *J. Phys. Chem. Lett.* **2014**, *5*, 3408−3414.
(57) Morales, E. H.; Martirez, J. M. P.; Saidi, W. A.; Rappe, A. M.; Bonnell, D. A. *ACS Nano* **2014**, *8*, 4465−4473.
(58) Martirez, J. M. P.; Morales, E. H.; Saidi, W. A.; Bonnell, D. A.; Rappe, A. M. *Phys. Rev. Lett.* **2012**, *109*, 256802.

DOI: 10.1021/acscatal.7b02761
ACS Catal. 2017, 7, 7718−7725

(59) Kim, S.; Schoenberg, M. R.; Rappe, A. M. *Phys. Rev. Lett.* **2011**, *107*, 076102.
(60) Kolpak, A. M.; Li, D.; Shao, R.; Rappe, A. M.; Bonnell, D. A. *Phys. Rev. Lett.* **2008**, *101*, 036102.
(61) Levchenko, S. V.; Rappe, A. M. *Phys. Rev. Lett.* **2008**, *100*, 256101.
(62) Kolpak, A. M.; Grinberg, I.; Rappe, A. M. *Phys. Rev. Lett.* **2007**, *98*, 166101.
(63) Li, Q.; Hu, X. *Phys. Rev. B: Condens. Matter Mater. Phys.* **2006**, *74*, 035414.
(64) Kanama, D.; Oyama, S. T.; Otani, S.; Cox, D. F. *Surf. Sci.* **2004**, *552*, 8−16.
(65) Moula, M. G.; Suzuki, S.; Chun, W.-J.; Otani, S.; Oyama, S. T.; Asakura, K. *Surf. Interface Anal.* **2006**, *38*, 1611−1614.
(66) Suzuki, S.; Moula, G. M.; Miyamoto, T.; Nakagawa, Y.; Kinosthita, K.; Asakura, K.; Oyama, S. T.; Otani, S. *J. Nanosci. Nanotechnol.* **2009**, *9*, 195−201.
(67) Guo, D.; Nakagawa, Y.; Ariga, H.; Suzuki, S.; Kinoshita, K.; Miyamoto, T.; Takakusagi, S.; Asakura, K.; Otani, S.; Oyama, S. T. *Surf. Sci.* **2010**, *604*, 1347−1352.
(68) Hernandez, A. B.; Ariga, H.; Takakusagi, S.; Kinoshita, K.; Suzuki, S.; Otani, S.; Oyama, S. T.; Asakura, K. *Chem. Phys. Lett.* **2011**, *513*, 48−52.
(69) Kucernak, A. R.; Sundaram, V. N. N. *J. Mater. Chem. A* **2014**, *2*, 17435−17445.
(70) Jin, L.; Xia, H.; Huang, Z.; Lv, C.; Wang, J.; Humphrey, M. G.; Zhang, C. *J. Mater. Chem. A* **2016**, *4*, 10925−10932.
(71) Edamoto, K.; Nakadai, Y.; Inomata, H.; Ozawa, K.; Otani, S. *Solid State Commun.* **2008**, *148*, 135−138.
(72) Falch, S.; Lamparter, P.; Steeb, S. *Z. Naturforsch., A: Phys. Sci.* **1984**, *39*, 1175−1183.
(73) Hohenberg, P.; Kohn, W. *Phys. Rev.* **1964**, *136*, B864−B871.
(74) Kohn, W.; Sham, L. J. *Phys. Rev.* **1965**, *140*, A1133−A1138.
(75) Giannozzi, P.; Baroni, S.; Bonini, N.; Calandra, M.; Car, R.; Cavazzoni, C.; Ceresoli, D.; Chiarotti, G. L.; Cococcioni, M.; Dabo, I.; et al. *J. Phys.: Condens. Matter* **2009**, *21*, 395502.
(76) Rappe, A. M.; Rabe, K. M.; Kaxiras, E.; Joannopoulos, J. D. *Phys. Rev. B: Condens. Matter Mater. Phys.* **1990**, *41*, 1227−1230.
(77) Ramer, N. J.; Rappe, A. M. *Phys. Rev. B: Condens. Matter Mater. Phys.* **1999**, *59*, 12471−12478.
(78) *Opium - pseudopotential generation project*. http://opium.sourceforge.net.
(79) Perdew, J. P.; Burke, K.; Ernzerhof, M. *Phys. Rev. Lett.* **1996**, *77*, 3865.
(80) Grimme, S. *J. Comput. Chem.* **2006**, *27*, 1787−1799.
(81) Ramalho, J. P. P.; Gomes, J. R.; Illas, F. *RSC Adv.* **2013**, *3*, 13085−13100.
(82) Eder, F.; Lercher, J. A. *Zeolites* **1997**, *18*, 75−81.
(83) Bengtsson, L. *Phys. Rev. B: Condens. Matter Mater. Phys.* **1999**, *59*, 12301−12304.
(84) Rong, X.; Kolpak, A. M. *J. Phys. Chem. Lett.* **2015**, *6*, 1785−1789.
(85) Chizmeshya, A.; Ritter, C.; Tolle, J.; Cook, C.; Menendez, J.; Kouvetakis, J. *Chem. Mater.* **2006**, *18*, 6266−6277.
(86) Cottrell, T. L. *The Strengths of Chemical Bonds*, 2nd ed.; Academic Press: London, 1958; p A21.
(87) Ledendecker, M.; Mondschein, J.; Kasian, O.; Geiger, S.; Göhl, D.; Schalenbach, M.; Zeradjanin, A.; Cherevko, S.; Schaak, R. E.; Mayrhofer, K. *Angew. Chem.* **2017**, *129*, 9899−9903.
(88) Kibsgaard, J.; Tsai, C.; Chan, K.; Benck, J. D.; Nørskov, J. K.; Abild-Pedersen, F.; Jaramillo, T. F. *Energy Environ. Sci.* **2015**, *8*, 3022−3029.
(89) Kibsgaard, J.; Jaramillo, T. F. *Angew. Chem., Int. Ed.* **2014**, *53*, 14433−14437.
(90) Cabán-Acevedo, M.; Stone, M. L.; Schmidt, J.; Thomas, J. G.; Ding, Q.; Chang, H.-C.; Tsai, M.-L.; He, J.-H.; Jin, S. *Nat. Mater.* **2015**, *14*, 1245−1251.
(91) Luo, J.; Wang, H.; Su, G.; Tang, Y.; Liu, H.; Tian, F.; Li, D. *J. Mater. Chem. A* **2017**, *5*, 14865−14872.
(92) Feng, L.; Vrubel, H.; Bensimon, M.; Hu, X. *Phys. Chem. Chem. Phys.* **2014**, *16*, 5917−5921.
(93) Pu, Z.; Liu, Q.; Tang, C.; Asiri, A. M.; Sun, X. *Nanoscale* **2014**, *6*, 11031−11034.
(94) Pan, Y.; Hu, W.; Liu, D.; Liu, Y.; Liu, C. *J. Mater. Chem. A* **2015**, *3*, 13087−13094.

DOI: 10.1021/acscatal.7b02761
ACS Catal. 2017, 7, 7718−7725